The role of electric field in microfluidic heating induced by standing surface acoustic waves

Tengfei Zheng,[1,2] Chaohui Wang,[1,2,a)] Qiao Hu,[2] and Shoupeng Wei[1]
[1]*State Key Laboratory for Manufacturing Systems Engineering, Xi'an Jiaotong University, Xian 710049, People's Republic of China*
[2]*Shaanxi Key Lab of Intelligent Robots, Xi'an Jiaotong University, Xian 710049, People's Republic of China*

(Received 19 March 2018; accepted 11 May 2018; published online 5 June 2018)

The heating mechanism of standing surface acoustic waves (SSAWs) on a $LiNbO_3$ substrate has been experimentally studied. Three devices with different substrates were used to heat the drops with NaCl concentrations ranging from 0 to 1 g/l, respectively. The device with a glass substrate was used to shield acoustic waves. The device with an Au layer between the $LiNbO_3$ substrate and the droplet was used to shield the alternating current field. The results show that the thermal effect induced by SSAWs on the $LiNbO_3$ substrate is composed of the acoustothermal effect due to SSAWs and the electric field thermal effect (Joule heat) due to the alternating current field. The electric field thermal effect which is ignored in SSAW devices previously plays an important role in the thermal effect induced by SSAWs. These results provide a meaningful insight into the mechanism of SSAW-based heating, which is of great help to guide the effective use of the SSAW-based heating technique for various applications. *Published by AIP Publishing.*
https://doi.org/10.1063/1.5030052

Standing surface acoustic waves (SSAWs) represent a very useful platform in applications of biotechnology and material engineering.[1–5] Examples of applications that SSAWs excel at are manipulating particles and[6] cells,[7] generating and controlling droplets,[8] and mixing,[9] atomizing,[10] or driving fluids on the micro-scale.[11] Within the wide context of digital microfluidics, the alternating current (AC) field induced by SSAWs is also used to pattern rod-shaped nanowires,[12] CNTs,[13,14] and particles.[15,16] However, SSAWs will heat the fluid in the process of manipulating fluid, particles, nanowires, and cells. High temperature may destroy the biological activity and alter material's properties. So, it is important to research the heating effect in SSAW-based microfluidics.

Although the heating effect is a much discussed issue in SSAW-based microfluidics and questions surrounding the problem of fluid heating are continually arising, to date, only a few studies investigated the thermal effect induced by SAWs in microfluidics. Characterization of the SAW-based liquid heating effect was first reported in 2005[17] and further expanded upon in 2009.[18] Ito *et al.* demonstrated that there was an association between the attenuation of a longitudinal wave and the temperature distribution.[19] To control droplet temperature changes, Shilton *et al.* investigated SAW-driven heating in digital microfluidic systems.[20] Park *et al.* proposed acoustothermal tweezers for the control of the droplet position, which is based on thermocapillary droplet migration actuated by acoustothermal heating.[21] Then, heating resulting from the SSAW thermal effect was used as an energy source for synthetic chemistry in digital microfluidics,[22,23] polymerase chain reactions (PCRs) in an oil-covered droplet,[24,25] controlling drug release from thermal sensitive liposomes,[26] disposable thermochromic displays,[27] and so on. In these experiments, the authors ascribed the thermal effect to radiated acoustic waves induced by SSAWs; however, they ignored the thermal effect resulting from the AC field. All authors paid attention to water and glycerin to demonstrate that the thermal effect induced by SSAWs was strongly dependent on input power and fluid viscosity and ascribed the temperature change to the viscous dissipation of the acoustic energy. However, as the standing surface waves (SSAWs) vibrate on the piezoelectric substrate, SSAWs induce a non-uniform charge distribution and create virtual electrodes on the piezoelectric substrate [as shown in Fig. 1(a)]. Therefore, the SSAW field and the electric field coexist in microfluidics. The droplet on the substrate is heated by standing waves and the AC field, respectively. It is difficult to study the law of thermal effect by ignoring the Joule heat, which limits the applications of SSAWs in common biotechnology fluid and material engineering, such as ionic liquid, blood, and so on.

Here, we investigate the heating mechanism in SSAW-based microfluidic systems. Three different devices [as shown in Figs. 2(b)–2(d)] are designed and fabricated to research the role of the AC thermal effect (Joule heat). The results demonstrate that the droplet heating in SSAW-based systems is composed of the acoustothermal effect and Joule heat. The Joule heat is related to solution electrical conductivity, and the acoustothermal effect is related to solution viscous dissipation. The Joule heat, which is ignored previously, plays an important role in SSAW-based microfluidics.

The devices are fabricated by patterning 100 nm thick gold with a 10 nm titanium adhesion layer onto substrates, via optical lithography. In Fig. 1(b), two nonweighted interdigital transducers (IDT and Au/Ti) are patterned on the surface of the single-crystal substrate (lithium niobate, $LiNbO_3$, LN). A droplet of 5 μl is placed on the surface between two IDTs to form the SSAW-based microfluidic system. The standing waves and the AC field co-exist, so the droplet is heated by standing waves and the AC field. In Fig. 1(c), two

a)Email: chhw@mail.xjtu.edu.cn

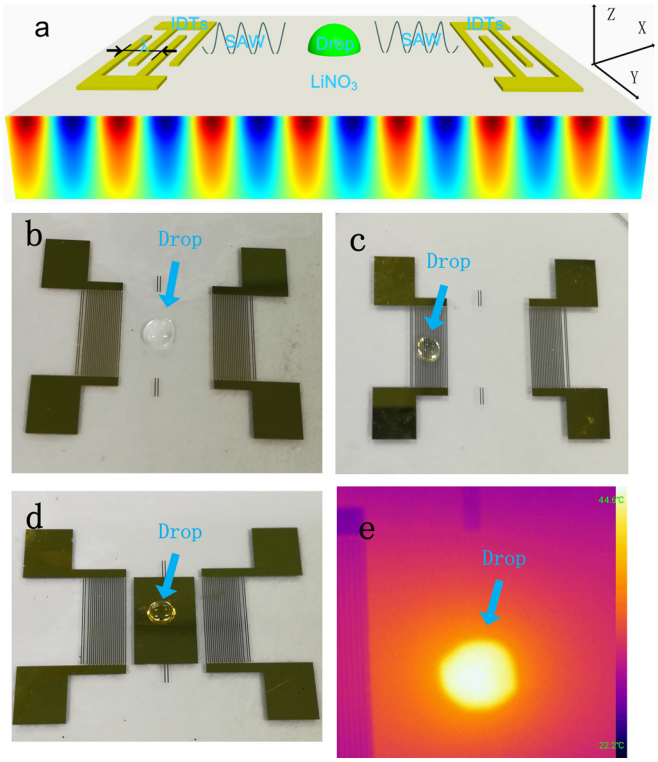

FIG. 1. (a) Two travelling surface acoustic waves generated by a pair of IDTs propagate toward the microdroplet. (b) SSAW device formed by depositing IDTs on the $LiNbO_3$ surface. (c) IDTs deposited on the glass surface. (d) SSAW device by inserting a layer of Au between the $LiNbO_3$ substrate and the droplet. (e) Infrared image obtained by the infrared camera.

nonweighted interdigital transducers (IDT and Au/Ti) are patterned on the glass surface. A droplet of 5 μl is placed on the IDTs and heated by the AC field. In Fig. 1(d), a gold plate and two IDTs are patterned on the $LiNbO_3$ surface. A droplet of 5 μl is placed on the surface of the gold plate to shield the droplet from the AC field. So, the droplet is heated by standing waves. The width of the IDT fingers is 50 μm. The center frequency in Figs. 1(b) and 1(d) is 17.5 MHz. An infrared camera (FOTRIC 226, USA) is used to measure the droplet temperature. The room temperature was 21 °C. The

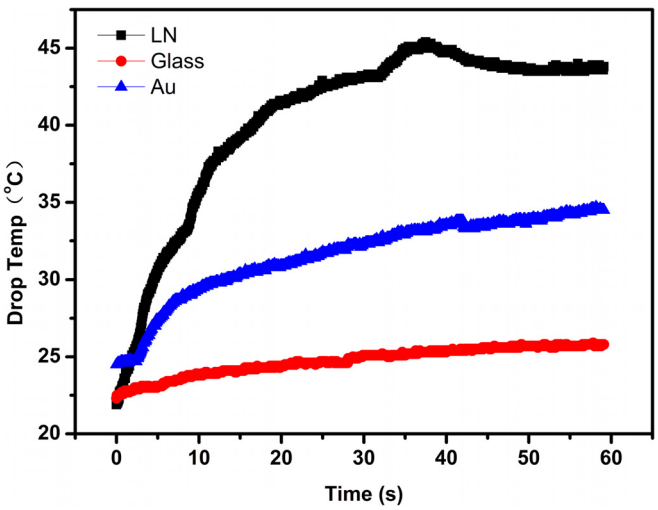

FIG. 2. The curves of the droplet temperature change on the $LiNbO_3$ substrate, glass substrate, and Au, when the sinusoidal signal was used to heat the deionized water drops.

moisture was 58%. Before measuring the droplet temperature, the camera was first used to measure the droplet temperature at room temperature. The droplet temperature was the same as the room temperature. Figure 1(e) shows the temperature of the deionized water droplet located on the $LiNbO_3$ surface.

In the experiments, the signal of 1 V is generated from an AC signal generator (Tektronix AFG3251C, USA) and amplified using a power amplifier (Amplifier research 75A 250A, USA). All four electrodes (2 electrodes on each of the IDTs) are connected to the RF output of the amplifier. The input power of SAWs is measured using a digital oscilloscope (Tektronix TDS3014B, USA) connected to the electrodes. Three devices [as shown in Figs. 1(b)–1(d)] are used to heat the 5 μl deionized (DI) water droplet to study the heating mechanism in SSAW-based microfluidic systems. In Fig. 1(b), the droplet is heated by standing waves and the AC field, and the maximum temperature is 43.5 °C (as shown in Fig. 2). In Fig. 1(c), the droplet is heated by the AC field, and the maximum temperature is 26 °C (as shown in Fig. 2). In Fig. 1(d), the droplet is heated by standing waves, and the maximum temperature is 34.5 °C (as shown in Fig. 2). The results in Fig. 2 demonstrate that the droplet temperature heated by standing waves and the AC field is higher than that heated by standing waves or the AC field, which implies that the thermal effect induced by SSAW is composed of the acoustothermal effect and Joule heat. In water, the heating induced by the electric field is smaller than that induced by acoustothermal effects, due to the low electrical conductivity of deionized water. The temperature in Fig. 2 increases with time until the temperature reaches the maximum temperature. When the devices were used to heat the droplet, the input power is applied continuously. The heating induced by the devices remains consistent all the time. However, the heat flux between the droplet and air increases with the increase in the droplet temperature.[28,29] When the heat flux between the droplet and air is smaller than the heating induced by the devices, the temperature increases with time. When the flux between the droplet and air is equal to the heating induced by the devices, the temperature reaches the maximum.

To further understand the heating mechanism in SSAW-based microfluidic systems, three devices [as shown in Figs. 1(b)–1(d)] are used to heat 5 μl microdroplets with varying sodium chloride (NaCl) concentrations(C) from 0 to 1 g/l separately. For changing little with the change in NaCl concentrations, the viscosity change of the NaCl solution can be ignored in this paper. Figure 3 shows the droplet temperature change, when the droplets are heated by the device in Fig. 1(b). The results demonstrate that the droplet temperature increases with NaCl concentration enhancement, while the NaCl concentration is lower than 0.1 g/l; the droplet temperature decreases with concentration enhancement, while the NaCl concentration is higher than 0.1 g/l. Figure 4 shows the droplet temperature change, when the droplets are heated by the device shown in Fig. 1(c). The results show that the variation tendency of droplet temperature change is similar to that in Fig. 3. However, the maximum temperature in Fig. 4 is higher than that in Fig. 3. In Fig. 3, the substrate of the device is LN (a kind of piezoelectric material). When input

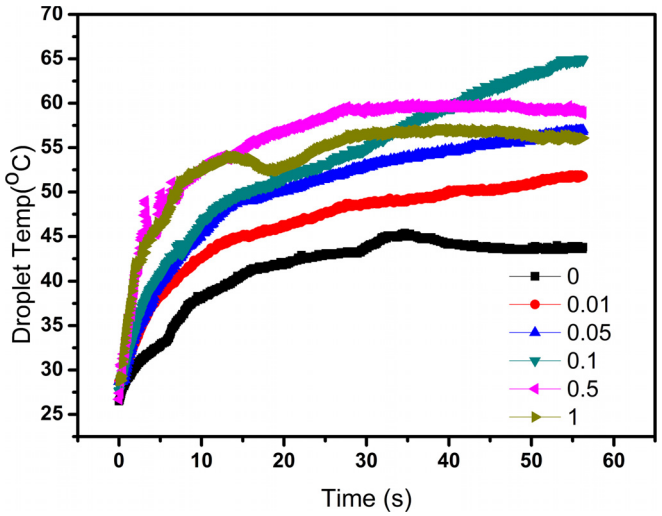

FIG. 3. The curves of the droplet temperature change on the $LiNbO_3$ substrate when the sinusoidal signal was used to heat the drops with NaCl concentrations ranging from 0 to 1 g/l separately.

power is applied, the waves propagate on the substrate. The area covered by the droplet is much smaller than the entire area. So, part of the input power is used to heat the droplet. In Fig. 4, the substrate is glass. When the input power is applied, almost all the power is used to heat the droplet. Besides, the heating induced by the electric field is larger than that induced by acoustothermal effects, for the ion solution. So, the maximum temperature in Fig. 4 is higher than that in Fig. 3. Figure 5 shows the droplet temperature change, when the droplets are heated by the device in Fig. 1(d). The droplet temperature change remains consistent and is lower than the droplet heated by the interaction of SSAWs and the AC field on the $LiNbO_3$ substrate.

The experimental results allow us to conclude that the thermal effect induced by SSAWs on the piezoelectric substrate is composed of the acoustothermal effect and Joule heat. According to the acoustothermal effect, a liquid droplet heating effect depends on the attenuation of the longitudinal wave in the droplet. The attenuation of the longitudinal wave is given by the relation as follows:[30]

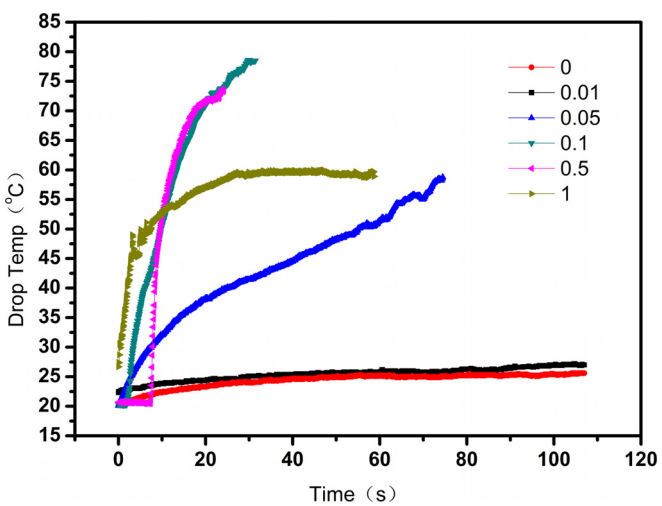

FIG. 4. The curves of the droplet temperature change on the glass substrate when the sinusoidal signal was used to heat the drops with NaCl concentrations ranging from 0 to 1 g/l separately.

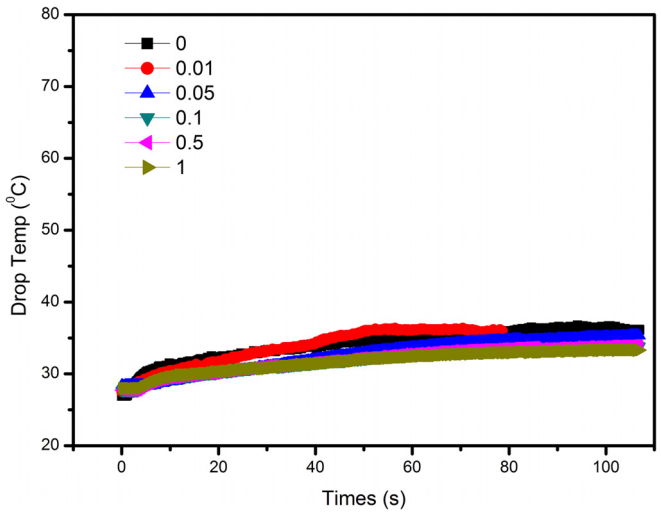

FIG. 5. The curves of the droplet temperature change on Au, when the sinusoidal signal was used to heat the drops with NaCl concentrations ranging from 0 to 1 g/l separately.

$$\alpha = R\omega^2/2c_L^3, \tag{1}$$

where R is denoted as

$$R = (1/\rho_L)(4\mu/3 + \mu' + K(\gamma - 1)/C_p), \tag{2}$$

where R is the dissipation coefficient, ω the angular frequency, c_L the velocity of the wave in the liquid, ρ_L the density of the liquid, μ the dynamic viscosity, μ' the volume viscosity, K the thermal conductivity of liquid, C_p the heat capacity at constant pressure, and γ the ratio of C_p/C_v with C_v being the heat capacity at constant volume. Because the ratio K/C_p will be low and close to zero, the last term can be neglected when calculating the attenuation. So, the acoustothermal effect is related to liquid viscosity. In Fig. 1(d), the droplet temperature change remains consistent (as shown in Fig. 5), which illustrates that the viscosity change of NaCl solution can be neglected. The temperature change in Fig. 5 is lower than that in Fig. 3, which suggests that the acoustothermal effect is just part of the SSAW thermal effect.

Taking the AC field thermal effect into consideration, a liquid droplet heating effect depends on the electrical conductivity. When the AC field frequency is lower than 300 MHz, the thermal effect resulting from the AC field is Joule heat. The heat transfer equation of the microdroplet can be given by the relation

$$\nabla \cdot (k_m \nabla T) + \sigma E^2 = 0, \tag{3}$$

where k_m is the thermal conductivity, σ is the electrical conductivity, and E is the electric field vector. The specific conductance of a solution containing one kind of electrolyte depends on the concentration of the electrolyte. So, the Joule heat (electric field thermal effect) is related to the concentration of the electrolyte. The droplet temperature change in Fig. 4 is similar to that in Fig. 3, which illustrates that the Joule heat induced by the AC field is also part of the SSAW thermal effect. In Figs. 3 and 4, there is a temperature peak at the concentration of 0.1 g/l. For a solution of a strong electrolyte at a low concentration, the conductivity is directly

proportional to the concentration. As a result, the droplet temperature increases with the NaCl concentration enhancement, when the NaCl concentration is lower than 0.1 g/l. As the concentration of the electrolyte solution increases above 0.1g/l, it is easy to form a salt skin in the process of evaporation. In devices (b) and (c), streaming is generated, when the input power is applied. Salt is formed in the droplet instead of in the droplet triple contact line.[31,32] A salt skin is formed between the droplet and the substrate. At the same time, the electric field exponential decreases with the increase in the distance. With the decrease in the electric field, the Joule heat decreases. So, the droplet temperature decreases with the NaCl concentration enhancement, when the NaCl concentration is higher than 0.1 g/l.

In summary, the mechanism of standing surface acoustic wave (SSAW) based heating is demonstrated. The standing waves and the electric field co-exist in the droplet inducing the acoustothermal and Joule heat. Three different devices were used to decouple Joule heat from the acoustothermal effect. It has been found that the Joule heat is related to solution electrical conductivity and the acoustothermal effect is related to solution viscous dissipation. The experiments show that the AC field thermal effect (Joule heat), which is neglected by researchers, plays an important role in the thermal effect induced by SSAWs. The results will help us to better understand the thermal effect induced by SSAWs and provide the foundation to precisely control the thermal effect, especially for that in ionic liquid and blood. As a result, the results will promote the applications of SSAWs in microfluidics, such as high stable control of chemical and biological reactions, performed using the complementary SSAW-driven process.

This work was supported by the National Natural Science Foundation of China (No. 51575441).

[1]H. Li, J. R. Friend, and L. Y. Yeo, Phys. Rev. Lett. **101**, 084502 (2008).
[2]C. Devendran, D. J. Collins, Y. Ai, and A. Neild, Phys. Rev. Lett. **118**, 154501 (2017).
[3]L. Shen and C. Wang, Phys. Rev. E **97**(3), 033103 (2018).
[4]M. Wu, Z. Mao, K. Chen, B. Hunter, Y. Chen, R. Joseph, L. Ren, P. Li, L. Wang, and T. J. Huang, Adv. Funct. Mater. **27**, 1606039 (2017).
[5]J. P. Lata, G. Feng, J. Guo, P. H. Huang, Y. Jian, and T. J. Huang, Adv. Mater. **28**, 8632–8638 (2016).
[6]A. Riaud, M. Baudoin, O. B. Matar, L. Becerra, and J.-L. Thomas, Phys. Rev. Appl. **7**(2), 024007 (2017).
[7]S. M. Naseer, A. Manbachi, M. Samandari, P. Walch, Y. Gao, Y. S. Zhang, F. Davoudi, W. Wang, K. Abrinia, and J. M. Cooper, Biofabrication **9**, 015020 (2017).
[8]H. J. Jin, D. Ghulam, P. Jinsoo, A. Husnain, P. Kwangseok, and H. J. Sung, Anal. Chem. **89**, 2211 (2017).
[9]G. Destgeer, S. Im, B. H. Ha, J. H. Jung, M. A. Ansari, and H. J. Sung, Appl. Phys. Lett. **104**(2), 023506 (2014).
[10]M. Baudoin, P. Brunet, O. Bou Matar, and E. Herth, Appl. Phys. Lett. **100**(15), 154102 (2012).
[11]L. Meng, F. Cai, J. Chen, L. Niu, and Y. Li, Appl. Phys. Lett. **100**(17), 173701 (2012).
[12]Y. Chen, X. Ding, L. S. C. Steven, S. Yang, P. H. Huang, N. Nama, Y. Zhao, A. A. Nawaz, F. Guo, and W. Wang, ACS Nano **7**, 3306 (2013).
[13]M. Morteza, A. Qi, L. Y. Yeo, and J. R. Friend, Adv. Funct. Mater. **25**, 1014–1023 (2015).
[14]Z. Qian, L. Li, H. L. Ma, J. Xu, Y. Fan, and H. Wang, Appl. Phys. Lett. **102**(21), 213106 (2013).
[15]T. F. Zheng, C. H. Wang, D. Niu, W. T. Jiang, Y. S. Shi, L. Yin, B. D. Chen, H. Z. Liu, and Y. C. Ding, RSC Adv. **4**(87), 46502–46507 (2014).
[16]Z. Ma, J. Guo, Y. J. Liu, and Y. Ai, Nanoscale **7**, 14047–14054 (2015).
[17]J. Kondoh, N. Shimizu, Y. Matsui, and S. Shiokawa, IEEE Trans. Ultrason. Ferroelectr. Freq. Control **52**, 1881 (2005).
[18]J. Kondoh, N. Shimizu, Y. Matsui, M. Sugimoto, and S. Shiokawa, Sens. Actuators A Phys. **149**, 292–297 (2009).
[19]S. Ito, M. Sugimoto, Y. Matsui, and J. Kondoh, Jpn. J. Appl. Phys., Part 1 **46**, 4718–4722 (2007).
[20]R. J. Shilton, V. Mattoli, M. Travagliati, M. Agostini, A. Desii, F. Beltram, and M. Cecchini, Adv. Funct. Mater. **25**, 5895–5901 (2015).
[21]J. Park, J. H. Jung, G. Destgeer, H. Ahmed, K. Park, and H. J. Sung, Lab Chip **18**(3), 422–432 (2017).
[22]K. Kulkarni, J. Friend, L. Yeo, and P. Perlmutter, Ultrason. Sonochem. **21**, 1305 (2014).
[23]K. Kulkarni, J. Friend, L. Yeo, and P. Perlmutter, Lab Chip **9**, 754 (2009).
[24]G. Xu, R. N. Gunson, J. M. Cooper, and J. Reboud, Chem. Commun. **51**, 2589 (2015).
[25]J. Reboud, Y. Bourquin, R. Wilson, G. S. Pall, M. Jiwaji, A. R. Pitt, A. Graham, A. P. Waters, and J. M. Cooper, Proc. Natl. Acad. Sci. U. S. A. **109**, 15162 (2012).
[26]L. Meng, Z. Deng, L. Niu, F. Li, F. Yan, J. Wu, F. Cai, and H. Zheng, Theranostics **5**, 1203–1213 (2015).
[27]J. Park, B. H. Ha, G. Destgeer, H. J. Jin, and H. J. Sung, RSC Adv. **6**, 33937–33944 (2016).
[28]G. Liang and I. Mudawar, Int. J. Heat Mass Transfer **106**, 103–126 (2017).
[29]J. C. Chen and K. K. Hsu, J. Heat Transfer **117**(3), 693–697 (1995).
[30]T. Rouxmarchand, D. Beyssen, F. Sarry, and O. Elmazria, IEEE Trans Ultrason. Ferroelectr. Freq. Control **62**, 729–735 (2015).
[31]Z. Tengfei, W. Chaohui, M. Baogang, and J. Zhuangde, CrystEngComm **18**, 6784–6788 (2016).
[32]C. Bai, C. Wang, T. Zheng, and Q. Hu, CrystEngComm **20**(9), 1245–1251 (2018).